A GLM/ICA ANALYSIS USING MOTION TRACKING AND ELECTROMYOGRAPHY DIFFERENTIATES BETWEEN BRAIN ACTIVATION DUE TO INTENDED AND UNINTENDED MOTIONS IN FNIRS IMAGES ACQUIRED DURING A FINGER TAPPING TASK PERFORMED BY CHILDREN WITH CEREBRAL PALSY

by

NATHAN HERVEY

Presented to the Faculty of the Graduate School of

The University of Texas at Arlington in Partial Fulfillment

of the Requirements

for the Degree of

MASTER OF SCIENCE BIOMEDICAL ENGINEERING

THE UNIVERSITY OF TEXAS AT ARLINGTON

May 2014

Acknowledgements

I would first like to thank Dr. George Alexandrakis for giving me the opportunity to work on this project and guiding me along the way. His advice has been invaluable, and I am grateful that I was able to work with such an excellent advisor. I would also like to thank Dr. Hanli Liu and Dr. Baohong Yuan for being on my committee, and for their helpful suggestions.

I would also like to give a special thanks to Bilal Khan who helped with every aspect of the project from the clinical measurements to the development of the method. Bilal has always been available to teach me something new or offer advice when I needed it, and he did so very often.

In addition I would like to thank Laura Shagman, Dr. Fenghua Tian, and the nursing staff at Texas Scottish Rite Hospital for their help with clinical measurements. I would also like to thank Kirsten Tulchin-Francis and everyone else in the movement science lab for their help with the acquisition and reconstruction of motion capture data.

Finally, I would like to thank my wife, Katie, and my parents, Terry and Sonya, for their constant love and support throughout my academic career.

April 14, 2014

Abstract

A GLM/ICA ANALYSIS USING MOTION TRACKING AND ELECTROMYOGRAPHY DIFFERENTIATES BETWEEN BRAIN ACTIVATION DUE TO INTENDED AND UNINTENDED MOTIONS IN FNIRS IMAGES ACQUIRED DURING A FINGER TAPPING TASK PERFORMED BY CHILDREN WITH CEREBRAL PALSY

Nathan Hervey, M.S.

The University of Texas at Arlington, 2014

Supervising Professor: George Alexandrakis

Functional neurological imaging has been shown to be valuable in evaluating brain plasticity in children with cerebral palsy (CP). In recent studies it has been demonstrated that functional near-infrared spectroscopy (fNIRS) is a viable and sensitive method for imaging motor cortex activities in children with CP. However, during unilateral finger tapping tasks children with CP often exhibit mirror motions (unintended motions in the non-tapping hand), and current fNIRS image formation techniques do not account for these motions. Therefore, the resulting fNIRS images contain activation from both intended and unintended motions. In this study, cortical activity was mapped with fNIRS on eight children with CP during a finger tapping task. Finger motion and arm muscle activation were concurrently measured using motion tracking cameras and electromyography (EMG). Subject-specific regressors were created from motion capture and EMG data, and independent component analysis (ICA) was applied to the ΔHbO time series data to create a new method, called GLM/ICA, to analyze fNIRS data. The motion regressors and independent components were used in a general linear model (GLM) analysis in an attempt to create fNIRS images representative of different motions.

The analysis provided an fNIRS image representing activation due to motion and muscle activity for each hand. In some cases the method removed mirror motion contaminations from activation images, and in other cases the image created for the mirror motions revealed interesting information not attainable with current analysis methods. Despite these positive results, the GLM/ICA method was only applicable to four out of eight subjects. Three of the recruited subjects did not have measurable mirror motions, one did not follow the protocol, and for one subject mirror motions were too correlated with the intended motions for the GLM/ICA method to be effective in some trials. Despite these limitations, this work demonstrates the feasibility and utility of the GLM/ICA method to help understand the contribution of mirror motions to fNIRS images from patients with motor deficits.

Table of Contents

List of Illustrations

List of Tables

Chapter 1

Introduction

1.1 Focus

The focus of this study was the development and application of a new method for the analysis of functional near-infrared spectroscopy (fNIRS) signals acquired during a hand tapping task performed by children with cerebral palsy (CP). FNIRS is a brain imaging method that uses near-infrared light to map changes in blood oxygen content in the cortex resulting from neuronal activation. FNIRS is relatively robust to motion artifacts, which is advantageous when mapping the brain activity of children with CP who exhibit unintended motions in one hand while attempting to tap with only the opposite hand. Nevertheless the presence of these unintended motions, commonly referred to as mirror motions, create neuronal activation that can overlap both spatially and temporally with the functional cortical regions activated by the intended hand motions. The goal of the method developed in this work was to separate the fNIRS signals created by the unintended hand motions from the intended ones and thus (a) clean up the brain activation map from mirror motion contaminations, and (b) simultaneously create a brain activation map created by the mirror motions that could shed light on how each subject compensates to achieve the intended tapping task. The key to the method developed here is the synchronous acquisition of fNIRS signals from the sensorimotor cortex along with electromyography (EMG) data from all major arm muscles for both arms as wells as motion tracking data of the fingers of both hands during tapping. The idea behind this synchronous multimodal data acquisition is that the EMG and motion tracking data could be used as regressors in a general linear model (GLM) of the fNIRS signals to thus provide a basis for separating brain activation signals created by intended versus mirror motions. The remaining of this chapter provides background information for the

developed method. Specifically, this chapter introduces the neurophysiology of motion control by the sensorimotor cortex, the pathology of CP, and provides some background on motion capture, EMG, fNIRS and GLM analysis. The last section of this chapter provides a brief outline of how in the subsequent thesis chapters this new fNIRS data analysis method was developed and tested using multimodal data acquired from children with CP.

1.2 Central Nervous System Physiology

Most human body motions are initiated in brain areas located in the cerebral cortex, which is the outermost layer of the brain [1]. The areas of the cortex involved in the planning and execution of motion are known collectively as the sensorimotor cortex and are shown in Figure 1-1. The primary motor cortex (M1) is located just anterior to the central sulcus, and it is primarily responsible for the execution of movements. When electrically stimulated, this area will elicit motion in different areas depending on the location of stimulation [1]. The homunculus, shown in Figure 1-2 relates each area of the primary motor cortex to the body part it controls. Notice that body parts which require finer motor control, such as the hand and fingers, have larger regions of the primary motor cortex devoted to their control, while parts like the shoulder and trunk, which don't require the same fine motor control, have smaller dedicated areas.

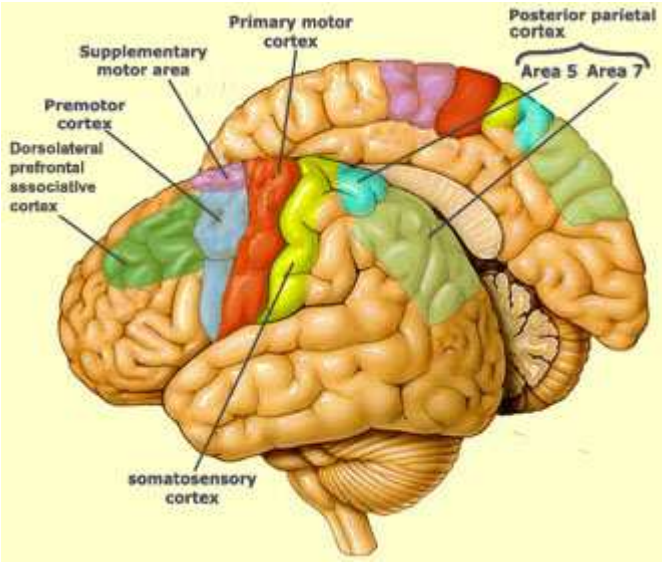

Figure 1-1 Areas of the cortex responsible for motion and sensation [2]

Although the primary motor cortex is essential for most movements, planning complex motions would not be possible without input from the other areas of the motor cortex. The posterior parietal cortex is active during the planning of motion and determines the body's position relative to external objects [1]. People with damage to this area of the brain often run into obstacles while walking and have difficulty locating objects even though they can accurately describe them [1]. The supplementary motor area (SMA) helps to coordinate quick sequences of motion and inhibit habitual motion when a different type of movement is required [1]. The premotor area is active right before motion, and integrates information about the desired target of the motion and the current position of the body [1]. The somatosensory cortex (S1) is located just posterior to the central sulcus, and it is the area primarily responsible for the sensation of touch. This area receives input from touch receptors, and similar to the primary motor cortex different locations of the somatosensory cortex are dedicated to receiving sensory information from specific areas of the body [1].

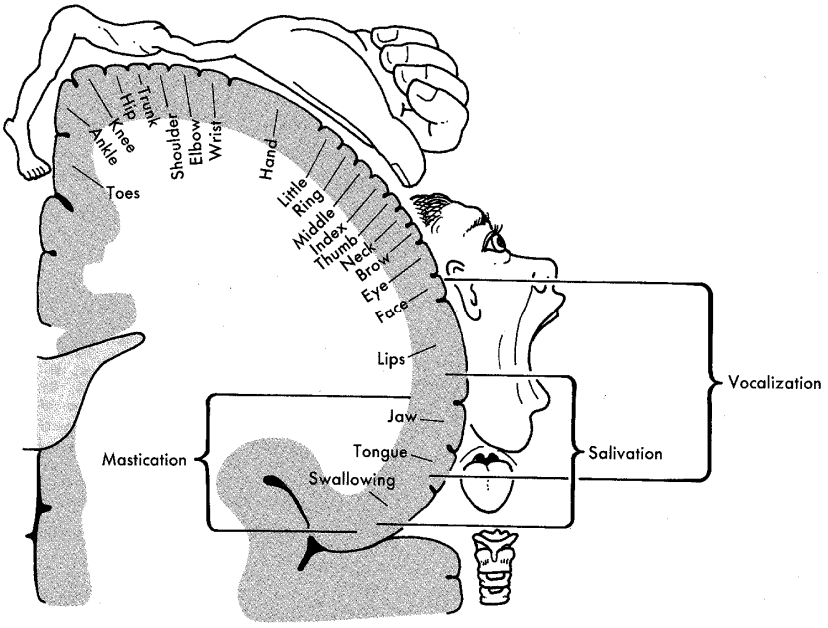

Figure 1-2 The homunculus, which shows the areas of the primary motor cortex responsible for different body parts [3]

After a movement is initiated in the motor cortex, the signal must be sent to the proper muscles. Nerve impulses are sent to the hands and fingers through the lateral corticospinal tract, which is a set of axons originating in the primary motor cortex and terminating at neurons in the spinal cord [1]. Figure 1-3 shows the path of the lateral corticospinal tract from the primary motor area (labeled pre-central gyrus in the figure) through the midbrain and medulla to the spinal cord. Notice that in the pyramids, which are nerve bundles located in the medulla, the axons cross to the opposite side of the spinal cord [1]. This results in the contralateral side of the brain controlling hand, finger, and many other peripheral motions. This point is crucial to understanding the disabilities caused by a brain lesion, as a lesion on the left side of the brain will cause right body impairment, and one of the right side will cause left body impairment.

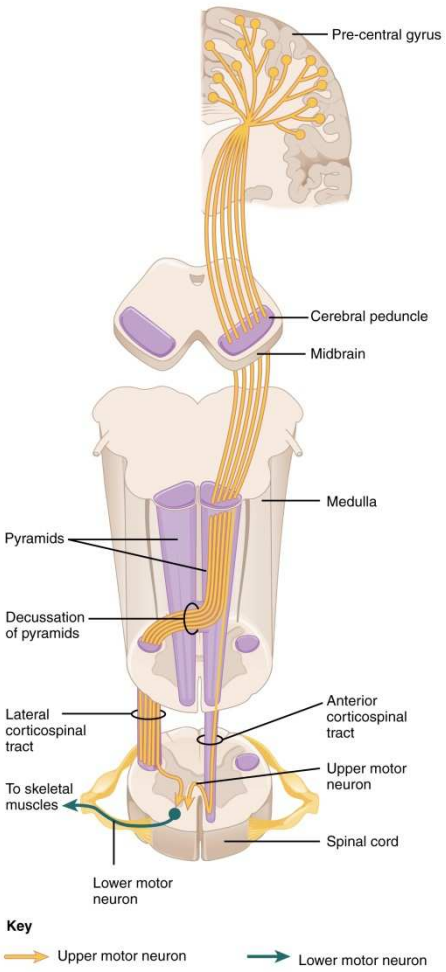

Figure 1-3 The corticospinal tracts [4]

1.3 Cerebral Palsy

Cerebral palsy (CP) is a group of movement and posture disorders that occurs in about 2.1 out of 1000 live births [5]. Disorders of movement and posture arise due to abnormalities in fetal or infant brain development resulting in the formation of lesions which can be located in the cortex and subcortical white matter [6]. In addition to impaired motor function, those with cerebral palsy may also experience a number of other neurological abnormalities including sensory disturbances, problems with cognition, and

seizures [7]. The degree of impairment can range from mild to severe, and a patient's functional abilities can be categorized using the Manual Ability Classification System (MACS) [8]. The MACS assesses a patient's ability to handle objects with both hands in his or her personal space [8]. Table 1-1 gives the description of each MACS level, with level 1 being the least severe and level 5 being the most severe.

Table 1-1 Description of MACS levels [8]

Level	Description
I	Handles objects easily and successfully. At most, limitations in the ease of performing manual tasks requiring speed and accuracy. However, any limitations in manual abilities do not restrict independence
II	Handles most objects but with somewhat reduced quality and/or speed of achievement. Certain activities may be avoided or be achieved with some difficulty; alternative ways of performance might be used but manual abilities do not usually restrict independence in daily activities.
III	Handles objects with difficulty; needs help to prepare and/or modify activities. The performance is slow and achieved with limited success regarding quality and quantity. Activities are performed independently if they have been set up or adapted.
IV	Handles a limited selection of easily managed objects in adapted situations. Performs parts of activities with effort and with limited success. Requires continuous support and assistance and/or adapted equipment, for even partial achievement of the activity.
V	Does not handle objects and has severely limited ability to perform even simple actions. Requires total assistance.

This study focuses on children with MACS I or II classifications that have hemiparetic cerebral palsy, which means lesions are only located on one side of the brain. This typically results in impaired movement on the contralateral side of the body with unimpaired movement on the ipsilateral side relative to the brain lesion. Subjects who have hemiparatic CP are known to have mirror motions when performing unimanual tasks [9]. In the context of the unimanual hand tapping used in this study, mirror motions are unintended motions in one hand while attempting to tap exclusively with the opposite hand. These aberrant motions pose a problem because current image formation techniques estimate the expected hemodynamic response based on correctly following

the experimental protocol and therefore cannot account for unintended motions. This may result in brain activation areas being attributed to intended motions when in fact they were due to the unintended mirror motions. This study introduces a new method which aims to solve this problem by incorporating motion capture data or EMG recordings into the analysis of fNIRS signals.

1.4 Functional Near-infrared Spectroscopy (fNIRS)

1.4.1 Neurovascular Coupling

An fNIRS imaging system is used to detect neuronal activity in the cerebral cortex, but it does not measure this activity directly. Instead it measures the changes in oxygenated hemoglobin (HbO) and deoxygenated hemoglobin (Hb) that occur due to neurovascular coupling, which is the correlation between neuronal activity and cerebral blood flow (CBF). The exact mechanisms by which neurovascular coupling occurs are still being investigated, and different theories have been proposed [10, 11]. However, despite the unknowns there is general agreement on the basic process of neurovascular coupling. The brain has small energy reserves, so it must be constantly supplied with glucose and oxygen which are used to make adenosine triphosphate (ATP), a form of energy [10]. When a neuron becomes active, demand for ATP increases because energy is required to restore the cell membrane to its resting potential after a nerve impulse is sent [11]. This results in increased CBF to the active neurons to replenish supplies of glucose and oxygen. In these active areas CBF increases more than oxygen consumption, which results in increased HbO concentrations and decreased Hb concentrations in the surrounding blood and tissue [11]. An fNIRS imaging system measures these changes to localize areas of neuronal activity in the cerebral cortex.

1.4.2 Principles of FNIRS

An fNIRS imaging system consists of fiber optic bundle coupled light sources and detectors which are placed on the scalp over the functional areas being measured. The source bundles emit near-infrared light with at least two distinct wavelengths approximately in the 700-900 nm wavelength range, and the detectors receive the back reflected light. Light propagation through biological tissue is influenced by two wavelength dependent parameters, the scattering coefficient μ_s' and the absorption coefficient μ_a. μ_s' represents the number of scattering events per unit length and μ_a the number of absorption events per unit length [12]. For biological tissue μ_s' is much larger than μ_a, which allows light propagation to be modeled as a diffusive process.

The absorption coefficient μ_a for most light wavelengths in tissue is relatively high resulting in a light transmission of only a few millimeters. However, an “optical window” exists in the 700-900 nm range where absorption is relatively low and light can propagate at distances up to 15 cm in brain tissue [13]. Within this window, the chromophores responsible for the majority of light absorption are HbO and Hb, and the absorption spectra for these and water are shown in Figure 1-4. Notice that the absorption spectra for HbO and Hb cross at around 810 nm, but are significantly different on either side of this value. By using one wavelength below and one above 810 nm, the relative changes in HbO and Hb concentrations can be determined by using the modified Beer-Lambert Law (MBLL).

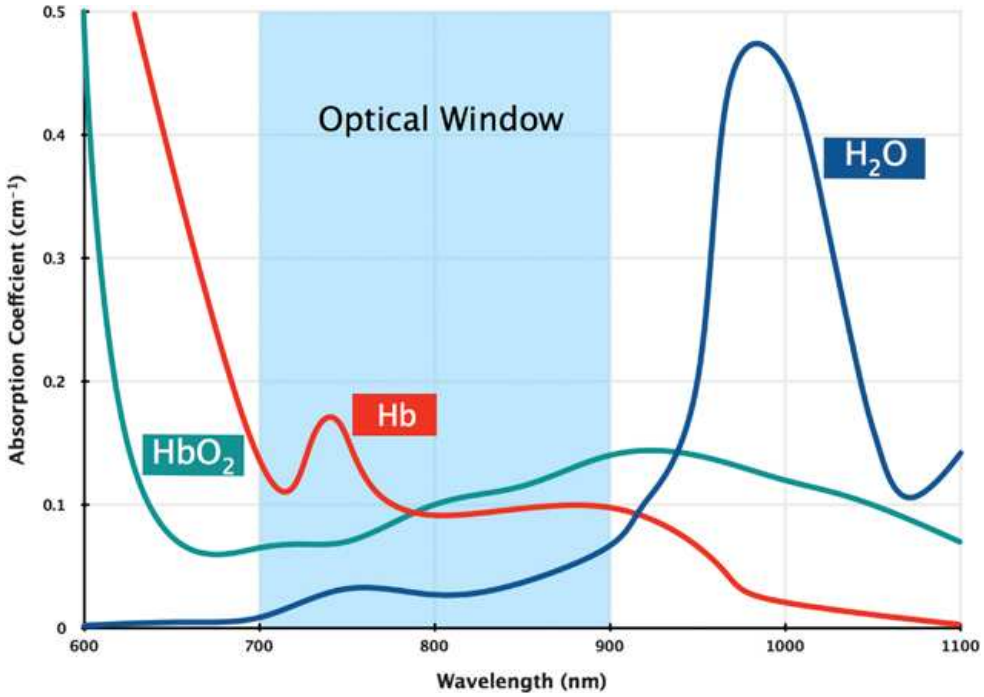

Figure 1-4 Absorption spectra for HbO, Hb, and water [14]

The MBLL provides a way to calculate the change in optical density (ΔOD). Equation 1.1 gives the MBLL [15]

$$\Delta OD = -\log\left(\frac{I}{I_0}\right) = \varepsilon * \Delta c * d * DPF \quad (1.1)$$

In equation 1.1, I_0 is the intensity of the light before the change in concentration, I is the intensity of the light after the change in concentration, ε is the molar extinction coefficient for the chromophore, Δc is the change in concentration of the chromophore, d is source-detector separation, and DPF is the differential path length equal to 6 cm, which is estimated when using a continuous wave system like the one used in this study [16]. To find the change in HbO and Hb, which are represented as ΔHbO and ΔHb, respectively, the MBLL can be written as a system of equations as given in equations 1.2 and 1.3 with L = d*DFP.

$$\Delta HbO = (\varepsilon Hb_{\lambda 2} * OD_{\lambda 1} - \varepsilon Hb_{\lambda 1} * OD_{\lambda 2})/(L * (\varepsilon Hb_{\lambda 2} * \varepsilon HbO_{\lambda 1} - \varepsilon Hb_{\lambda 1} * \varepsilon HbO_{\lambda 2})) \quad (1.2)$$

$$\Delta Hb = (\varepsilon HbO_{\lambda 2} * OD_{\lambda 1} - \varepsilon HbO_{\lambda 1} * OD_{\lambda 2})/(L * (\varepsilon Hb_{\lambda 1} * \varepsilon HbO_{\lambda 2} - \varepsilon Hb_{\lambda 2} * \varepsilon HbO_{\lambda 1})) \quad (1.3)$$

The MBLL allows the determination of changes in HbO and Hb in the cortex related to neurovascular coupling. Detecting these changes is necessary but not sufficient to distinguish active areas from non-active areas. A statistical approach, the general linear model (GLM), is used to analyze the changes in HbO to determine in which cortical regions have significantly higher amplitude hemodynamic fluctuations compared to background fluctuations occurring during the resting state. Background fluctuation in fNIRS signals are caused by cardiac pulsation, respiration, and Mayer waves [17-19]. Typically, cardiac pulsation is in the 0.8 Hz to 2.0 Hz range, respiration is in the 0.1 Hz to 0.3 Hz range, and Mayer waves are at frequencies below 0.1 Hz [20, 21]. Next, motion capture technology and EMG will be discussed, followed by a description of the GLM.

1.5 Motion Capture

1.5.1 Motion Capture Camera Systems

Motion capture is used in a variety of fields including music, dance, gesture recognition, medicine, biomechanics, and special effects for films [22]. In this study, an optical motion capture system with passive markers was used. These systems typically employ several cameras surrounding the subject being tracked to avoid marker occlusion and dropout. Motion is captured using retroreflective markers placed on the subject that reflect light provided by a source near the cameras. Light from the markers is projected onto the image plane (typically a CCD sensor), and each marker's centroid can be calculated in pixel coordinates. A projection matrix containing intrinsic and extrinsic camera properties can be defined to relate real world spatial coordinates to pixel coordinates [23]. This projection matrix can be found by calibration with an object with

known marker separations. Three dimensional real world coordinates can then be reconstructed using triangulation with data from at least two cameras.

When reflective markers are placed on the fingers motion capture systems can usually detect mirror motions during hand tapping tasks if they are present. However, in some cases a subject may press their resting hand against the table rather than visibly moving it thus suppressing these motions. To enable detection of these suppressed mirror movements EMG of all major arm muscles was performed synchronously with the motion tracking.

1.5.2 Electromyography (EMG)

EMG is the recording of electrical activity in the muscles. Before muscle contraction takes place, action potentials must travel through somatic motor pathways, which consist of neurons that originate in the central nervous system and terminate at skeletal muscles [24]. When an action potential reaches the axon terminal, acetylcholine is released into the synaptic cleft and binds to nicotinic receptors causing the muscle cells to depolarize. This depolarization triggers another action potential and causes the muscle cells to contract [24]. By placing electrodes on the surface of the skin, EMG records the electrical activity that occurs during muscle contraction. These recordings can then be used to determine when muscles were and were not active.

1.5.3 Concurrent Acquisition of Multimodal Kinetic Data during Brain Imaging

Previously motion capture or EMG has not been used in fNIRS studies on patients with disabilities. However, motion capture has been used in at least two fMRI studies, one with Parkinson's patients and another with a stroke patient, in an attempt to account for unintended motions [25, 26]. In both studies the incorporation of motion data helped identify active brain areas indicating that motion capture may be a valuable addition to function neuroimaging. EMG has also been used in fMRI studies in a similar

way. In one fMRI study with healthy patients EMG was used to record muscle activity during ankle contraction. Incorporation of the EMG data in the analysis resulted in more active voxels compared to the standard analysis [27]. Another study performed on patients with familial cortical myoclonic tremor with epilepsy showed that using EMG data in the analysis allowed the detection of brain activation due to involuntary motions that were not detected using the standard technique [28].

The aforementioned studies indicate that including data from motion capture or EMG has the potential to improve functional neuroimaging analysis techniques. The current standard technique, the GLM, uses a regressor created from the convolution of a standard HRF and a boxcar function, which indicates whether or not the stimulus is present. In a motor task, a subject may not always correctly follow the protocol, especially if a disability prevents him/her from doing so. In these cases the boxcar regressor does not accurately represent the performed task and may not produce desirable results. A regressor that better represents the patient's actual motion can often be made using motion capture or EMG and be used in a GLM analysis to produce better results.

1.6 The General Linear Model (GLM)

The GLM has traditionally been the standard method to analyze data in functional magnetic resonance imaging (fMRI), which is a widely used functional imaging technique with standardized methods of analysis [29]. Similar to fNIRS, fMRI measures changes in blood flow due to neurovascular coupling, so the GLM can also be used to analyze fNIRS data, as several studies have shown [30-32]. The GLM expresses a dependent variable, in this case changes in HbO over time, as a linear combination of reference functions. The basic GLM equation is given below [33] in equation 1.4.

$$\boldsymbol{Y} = \boldsymbol{X\beta} + \boldsymbol{e} \tag{1.4}$$

In equation 1.4, *Y* is a t x p matrix containing the measured HbO time series for each image pixel with t time points and p pixels. *X* is a t x n design matrix containing n regressors which attempts to model the expected changes in the HbO time series in *Y*. *β* is an n x p matrix of beta weights that indicates a regressor's level of contribution to explaining the measured HbO time series, and e is the model error, which is the variation in the HbO time series not explained by the regressors.

In general, the design matrix *X* will contain a column of ones to account for baseline activation, a regressor modeling the expected hemodynamic response for each experimental condition, and possibly other regressors to explain additional variations in the HbO time courses unrelated to the stimulus. Typically, regressors for the prediction of hemodynamic responses are created by convolving a standard hemodynamic response function with a boxcar time series that has a value of 1 when the stimulus is present and 0 when it is not [29]. A standard hemodynamic response function is the expected change in HbO due to a short duration stimulus, and its shape is typically modeled using gamma functions, but Poission and Gaussian functions are also used [29].

After measuring changes in HbO and creating the design matrix, the β estimates are found using ordinary least squares. This method assumes that all pixels and time point data are independent of each other and have constant variance [29]. These assumptions do not actually hold for fNIRS measurements, but meaningful results can still be attained using the GLM. Once the beta values have been computed they are used in a t-test to determine if significant activation is present in individual pixels for any of the experimental conditions. The details of this test are further explained in the methods section.

One limitation of the GLM is in the creation of the regressors for the design matrix. When performing experiments involving motion the convolution of a HRF with a

boxcar time series assumes that the subject correctly followed the protocol. This assumption is typically valid when working with healthy adult subjects who are capable of correctly following the protocol. However, it is often desirable to work with patients who have some disability, such those who have had a stroke, or in the case of this study children with cerebral palsy. In these cases it is not always possible for the subject to correctly perform the desired protocol. When this occurs, convolution with the boxcar function may create a regressor that is no longer indicative of the actual motions executed by the subject.

A few recent studies in the fMRI field have employed motion capture technology as a means to account for unintended patient motions in activation images by creating regressors with motion data instead of the standard boxcar function [25, 26]. One study performed on a stroke patient used a camera system to record movements during an ankle moving task, and concluded that using motion tracking helped to evaluate motor recovery by increasing the size and statistical significance of activation areas in brain images. [25] Also, a study with Parkinson's disease patients using a motion capture glove during a hand tapping task was able to better detect brain response to the drug levodopa compared to standard fMRI analysis.[26] Both studies provide evidence that functional brain imaging can be improved with motion capture technology. However, the issue of accounting for these unintended contributions in fNIRS images has not been addressed in prior work to date.

In this study an fNIRS imaging system is used to measure cortical hemodynamics while children with CP perform unimanual hand tapping tasks. For the children who exhibited mirror motions, subject specific regressors were created using motion capture or EMG data collected during the experiment. One regressor was created from the intended motions and another from the unintended motions and used in a GLM

analysis resulting in a separate image for each motion. Because the hemodynamic changes recorded by the fNIRS system were a mixture of the activation caused by each motion, an Independent Component Analysis (ICA) step was added to the HbO time series data analysis process, before incorporating them into the GLM.

1.7 Independent Component Analysis (ICA)

ICA is a statistical method useful in signal processing and data analysis. ICA was originally developed to solve problems similar to the "cocktail party problem" in which two people are speaking in a room with two microphones in different locations recording their speech [34]. Naturally, one may want recover the speech of the individual speakers using the mixed signals recorded with the two microphones. ICA provides a way to estimate the signals produced from different sources using only the recorded mixed signals by assuming that the sources are statistically independent at each time point. The ICA equation is given below in equation 1.5 [34].

$$x = \boldsymbol{A}s \tag{1.5}$$

In equation 1.5, *x* is a vector containing the measured mixed signals, *s* is a vector containing the sources, and *A* the mixing matrix which contains unknown parameters. For the purposes of ICA, it assumed that each mixture x_i and each source s_i is a random variable, and that all sources have nongaussian distributions. The sources, which are also the independent components, can be found using equation 1.6 [34].

$$s = \boldsymbol{W}x \tag{1.6}$$

In equation 1.6, W is the inverse of the mixing matrix A. It can be shown that by maximizing the nongaussianity of w^Tx, where w is one of the rows W, w^Tx gives an independent component [34]. For this study, the FastICA algorithm provided by researchers at the Helsinki University of Technology was used to estimate independent components [34]. The FastICA algorithm is a fixed-point algorithm that uses negentropy,

a measure of nongaussianity, to maximize the nongaussianity of $w^T x$ and estimate the independent components [34].

Some ambiguities exist in the estimated independent components. First, the variance and the sign of the components cannot be determined. An estimated component could be multiplied by -1 and still be valid. Also, the order of the components cannot be determined. Since A and s are both unknown, their terms could be rearranged giving a different order to the independent components [34].

In addition to the “cocktail party problem”, ICA has been applied in areas such as electroencephalography (EEG) data analysis and feature extraction in audio and images [34]. ICA has also found several uses in the evaluation of fNIRS data. In one study researchers were able to remove a skin blood flow artifact and more clearly show brain activation using ICA [35]. Similarly, other researchers have used ICA to reduce noise in fNIRS signals and increase statistical significance in activation areas [36]. ICA has also been used to characterize temporal and spatial features of brain activity and distinguish between different brain activations in a visual stimulus experiment [37]. ICA has also proved to be a reliable way to create resting state functional connectivity maps in the sensorimotor cortex [38].

In this study ICA is used to extract hemodynamic signals in fNIRS data collected during a finger tapping task. The independent components are used in a GLM analysis with subject specific kinematic regressors to determine which components are significantly correlated with intended and unintended motions. Brain activation images are created using the components found to be significant for each motion type.

1.8 Study Overview

In this study a new method is proposed for the analysis of fNIRS data acquired during a hand tapping task performed by children with CP. Chapter 1 has described the

relevant background information required to understand the methodology of the new GLM/ICA analysis technique. Next, chapter 2 discusses the subjects and the experimental protocol and setup. It then describes in detail how the new method was developed and applied to the experimental data. Chapter 3 first discusses which data sets were eligible for the GLM/ICA methods, and why many data sets were not eligible. Next, chapter 3 describes the positive results obtained by using the method on five data sets, and the negative results obtained for three data sets. A comparison of regressors made with motion capture and EMG data is then made, and the overall trends and limitations are discussed. Finally, Chapter 4 discusses the conclusions and future work of the study.

Chapter 2

Methods

2.1 Subjects

Eight hemiparetic cerebral palsy subjects were included in the study (6 male and 2 female, 10 ± 1.7 years old). Five patients had left arm hemiparesis and three had right arm hemiparesis. Two patients were classified as MACS 1 and six as MACS 2. Table 2-1 below contains detailed information for each patient, including the dates on which the measurements took place. Each subject was measured one week before, one week after, and six months after undergoing physical therapy with the exception of Subject 4 who did not return for the six month visit.

Table 2-1 Subject Information

Subject	Age	MACS	Gender	Hemiparesis	Visit 1	Visit 2	Visit 3
1	11yrs	1	M	Left	06/09/12	06/27/12	12/12/12
2	11yrs	2	M	Right	06/06/12	06/25/12	12/12/12
3	12yrs	2	M	Left	06/08/12	06/28/12	12/19/12
4	11yrs	1	M	Right	06/08/12	06/28/12	-
5	8yrs	2	M	Left	06/10/13	07/02/13	12/31/13
6	8yrs	2	F	Left	06/13/13	07/01/13	12/30/13
7	11yrs	2	F	Left	06/14/13	07/10/13	12/31/13
8	8yrs	2	M	Right	06/14/13	07/02/13	12/30/13

2.2 Experimental Protocol and Setup

2.2.1 Protocol

Each subject performed a finger tapping task, once with their dominant hand and once with their non-dominant hand, while the other hand was to remain at rest to the best of the subject's ability. During all tasks children were instructed to tap only with four fingers (excluding the thumb), in unison and keep their wrists on the table while finger tapping. Children were prompted to tap at a frequency of 1 Hz by following a program with an engaging animation made on Adobe flash (Adobe Systems Incorporated, San Jose, CA) in-house. The experimental protocol for finger tapping by each arm consisted of eight 15 s tapping periods, each followed by 25 s of rest, with a 3 minute rest period before the first tapping period only on the first trial.

2.2.2 Motion Capture and EMG

For the motion tracking of hands and arms during the finger tapping task 5 mm diameter hemispherical retroreflective markers (B&L Engineering, Santa Ana, CA) were attached with tape on the finger nail bed and just above the proximal interphalangeal joint on each finger, excluding the thumb as seen in Figure 2-1a. For the June 2012 tests the 3-d coordinates of these retroreflective markers were tracked by a six-camera VICON Mx motion capture system (Vicon, Denver, CO) at a sampling rate of 120 Hz. The approximate spatial arrangement of cameras relative to the subject is shown in Figure 2-1b. The cameras were 2-4 m above the floor (height varied) and had an approximate distance of 2 m from each other. The study was moved to a smaller room for the December 2012 and all the 2013 measurements where seven Vicon cameras were used. Figure 2-1c shows the approximate location of these cameras. The two cameras to the right and left side of the subject were approximately 1.5 m above the floor, the four cameras in the back were placed on the top of a cabinet about 3m above the floor, and

the final camera was placed in the cabinet at about 2 m above the floor. Muscle movement was monitored by eight sets of wireless EMG electrodes (BTS FREEEMG 300, BTS, Garbagnate Milanese MI, Italy) placed on the finger flexor and extensor muscles, biceps, and triceps of both arms.

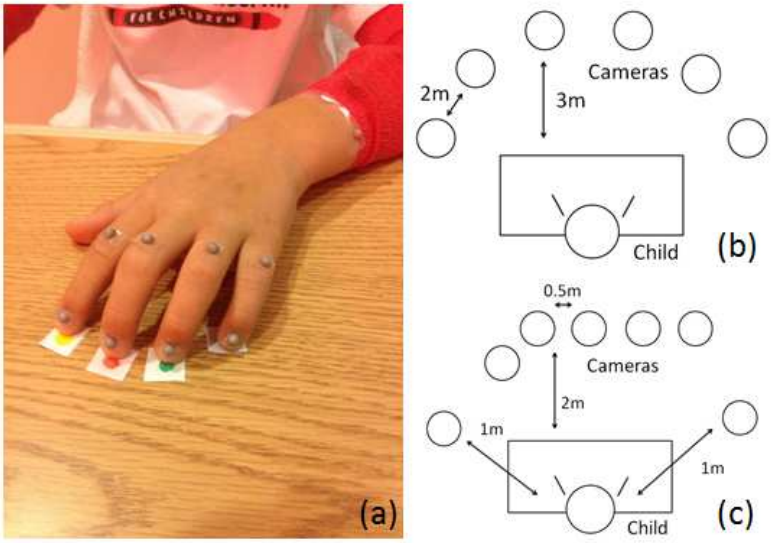

Figure 2-1 Motion tracking set-up (a) marker location on hand (b) camera placement for June 2012 (c) camera placement for December 2012 and all 2013

2.2.3 FNIRS Set-up

To measure ΔHbO in the sensorimotor cortex during the finger tapping protocol a continuous wave fNIRS system (CW-6, Techen Inc., Milford, Massachusetts) was used. A custom headset was created and affixed to the children's heads using Velcro. The source and detector locations are shown in Figure 2-2 where pink circles indicate sources and blue squares indicate detectors. Sixteen source bundles (each with two lasers) and thirty-two detectors were centered around the Cz position of the EEG International 10/20 system [39] and covered the pre-motor cortex (PMC), supplementary motor area (SMA), and primary motor sensory area (M1/S1). Each source bundle simultaneously emitted

690 nm and 830 nm light, which was received by up to six detectors located within a 3 cm radius. Each detector received light from up to three sources, with 8 short (1.5 cm) source-detector pairs used to measure background ΔHbO in the scalp. These signals were used to adaptively filter the fNIRS data (details in the next section). The geometry in Figure 2-2 gave a total of 84 source-detector pairs for each wavelength. The CW-6 detectors sampled at a rate of 25 Hz, and the system utilized frequency modulation (6.4 – 12.6 kHz, with 200 Hz increment) to simultaneously monitor activation over all source-detector pairs for the duration of the trial. Data acquisition for the fNIRS, EMG, and motion tracking systems was manually started simultaneously at the beginning of each measurement protocol, which afforded a synchronicity of ±0.5 s between modalities that is much shorter than the duration of elicited hemodynamic responses.

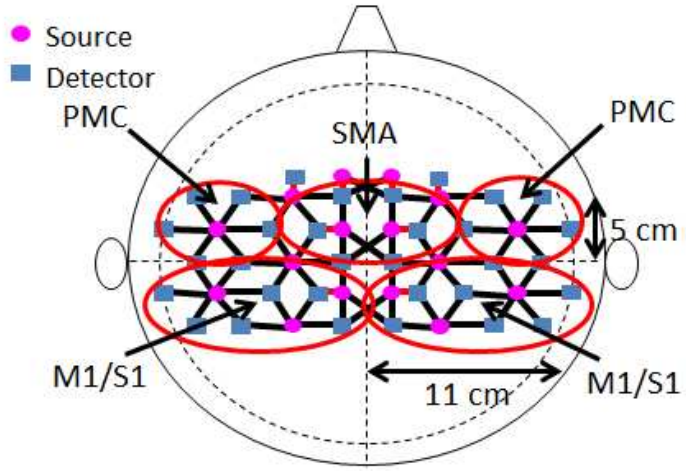

Figure 2-2 Source-detector geometry with covered cortical areas PMC (pre-motor cortex) SMA (supplementary motor area), and M1/S1 (primary motor/sensory area) circled

2.3 Signal Processing

2.3.1 FNIRS Signal Processing

First, fNIRS signals were band pass filter at from 0.01 to 0.4 Hz. Next, an adaptive filter using a least mean square algorithm was applied to the fNIRS signals to remove physiological noise [40]. Next, fNIRS signals from each tapping and resting block were visually inspected using the freely available Homer software package [41]. Any blocks containing motion artifacts were removed, and images were reconstructed using Homer, which uses a Moore-Penrose inversion scheme[42]. Files were then saved in the .hmr format and loaded into MATLAB. The saved Homer file provides the inverse of the sensitivity matrix and the changes in optical density for both wavelengths. By multiplying these together for each wavelength an image was reconstructed giving the change in optical density for each pixel. ΔHbO was then calculated for each pixel at each time point using equation 1.2.

2.3.2 Motion Tracking and EMG Signal Processing

Signal processing of motion capture data was performed in MATLAB. The motion capture system returned the 3-d position coordinates of the targets in mm in relation to a calibration coordinate system. This data was filtered using a low pass Butterworth filter at 7 Hz to eliminate high frequency noise present in the signal.

The EMG analysis began by band-pass filtering the EMG signals between 20 - 200 Hz. These signals were then full-wave rectified and low-pass filtered at 6 Hz giving a linear envelope of the muscle activity. Each envelope represented an individual finger tap.

2.4 Standard GLM Analysis

Most current fNIRS studies use a boxcar pattern as the time series representation of the finger tapping protocol[30] because no concurrent recording of the tapping pattern that was actually performed is available. Therefore in this work a standard boxcar fNIRS image was formed using GLM analysis for all cases to provide a basis of comparison for the fNIRS images formed by our proposed GLM/ICA method. For the boxcar based analysis a standard two-regressor GLM was used as shown in equation 2.1.

$$Y = \boldsymbol{X_0}\boldsymbol{\beta_0} + \boldsymbol{X_1}\boldsymbol{\beta_1} + \epsilon \quad (2.1)$$

In equation 2.1, Y represents a column matrix containing the measured hemodynamic response time series, concatenated by pixel (20 x 21 pixels) and ε represents the model error. The *X*'s represent the regressors, which model the expected hemodynamic response. In this case, X_0 was simply a column of ones, which models the baseline activation, or DC value, and X_1 represented a regressor that is a boxcar function coinciding with the experimental protocol (value of 1 when tapping, 0 when resting) convolved with a hemodynamic response function (HRF). The HRF, which modeled the predicted hemodynamic response per tap, was assumed to be a sum of six gamma functions[43]. The β's in equation represent the unknown predictor coefficients, which were computed using ordinary least squares [44]. Though generally not true for the low spatial resolution fNIRS images, the GLM method assumed that all pixels and time point data were independent from each other, and that their variance were constant[44]. The β1 estimate was then multiplied by the corresponding regressor to determine a ΔHbO concentration for each pixel in fNIRS images that were reconstructed at the 25 Hz data sampling rate. These time series values (except those excluded due to motion artifacts) were subsequently averaged into a single 40 s tapping/rest block per pixel. Time-

averaged ΔHbO activation images were finally formed by the time averaged pixel data within a 5 -15 s window relative to the beginning of each 40 s tapping/rest block.

2.5 The GLM/ICA Method

2.5.1 Overview

A flowchart for the overall process of the GLM/ICA method is given in Figure 2-3. Figure 2-3 is color coded to match Figure 2-5, which is included at the end of this chapter and gives a more detailed description of the GLM/ICA method. A general overview is given in this section, but each box is discussed in more detail in the next sections with the exception of the signal processing boxes which were discussed in section 2.3.2. After processing the motion capture or EMG data, motion regressors were created by convolving these time series data with the canonical HFR described previously. The overall goal was to use these patient specific regressors as a means to identify what part of the recorded fNIRS signal corresponded to the intended tapping motions and what part corresponded to unintended mirror motions. As a result, two fNIRS images were created for each data set, one for tapping and one for mirror motions, to thus assess their relative contributions to the overall activation patterns observed. To that end, a GLM was created with simultaneous regressors for both tapping and mirror motions. The fNIRS signals were subsequently reconstructed as an image using a standard Moore-Penrose inverse approach[42] then analyzed into independent components (ICs) by a FastICA algorithm[34]. ICs found to be significant using the GLM were categorized into one of three groups, one for tapping motion, one for mirror motion, and one for cross-talk. The ICs for the finger and mirror groups were summed using matrix multiplication, while the cross talk ICs were discarded. Subsequently, a final GLM was run for the finger and

mirror ICs to make an activation image for each motion. The next few sections give a detailed description of how this ICA/GLM algorithm was implemented.

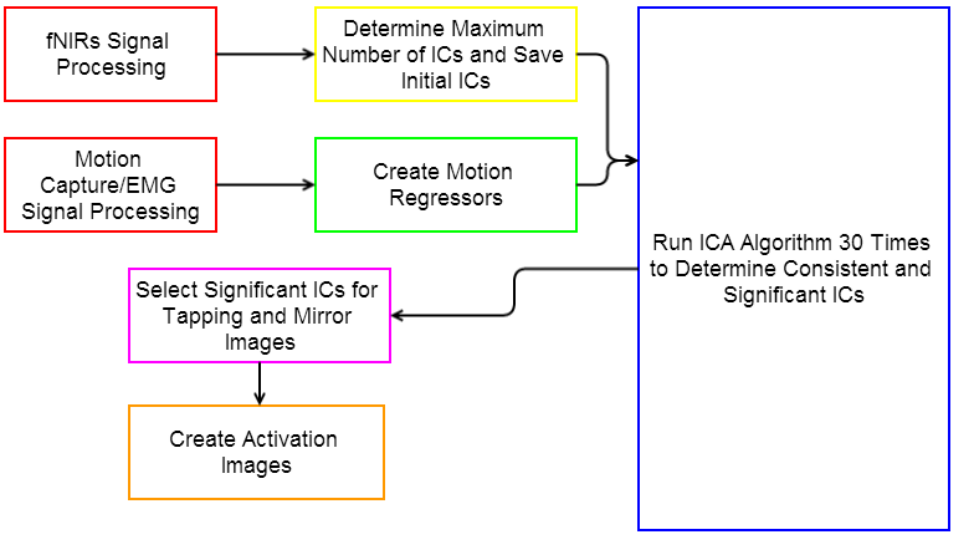

Figure 2-3 Overview of the GLM/ICA method

2.5.2 Creation of Motion Regressors

The goal of the GLM/ICA method is to provide more informative activation images by attributing brain activation during hand tapping tasks to either the intended motions in the active hand or unintended motions in the opposite mirror hand in children with cerebral palsy. To achieve this goal, information about the child's motion must be incorporated into the data analysis. Two subject specific kinematic regressors were created for each trial, one using data from the tapping and one from the mirror hand. Due to the nature of the tapping task, the largest amplitude changes were seen in distal markers located on the finger nails (see Figure 2-1a). Finger tapping occurred in a vertical direction relative to the table surface. For this reason, only the vertical trajectories of the distal markers were included in the creation of the regressors.

To use the kinematic regressors in the GLM the data must be continuous in time for the entire trial. In cases where continuous data was available for all distal markers, all these trajectories were used. However, in many cases continuous data was not available for all distal markers. In these cases only the markers with continuous data were used, which could be as few as one or as many as three. In the event that all distal markers contained small data gaps, an attempt was made to fill these gaps in certain situations where reasonable approximations could be made. In some trials gaps were only present during rest periods due to the subject moving his or her hand out of the field of view. In these cases the gaps were filled with a constant value since the subject was not moving during this period. In other cases the subjects tapped their hands so high that the distal markers left the cameras' field of view resulting in gaps at the apex of each tap. In these cases the gaps were filled with a cubic spline interpolation using the spline function in MATLAB. If large data gaps were present the trial had to be excluded. However, in all these cases there were either no mirror motions, or the fNIRS data contained significant motion artifacts, so the trials could not have been used anyways.

After filling any small gaps and selecting the appropriate marker trajectories based on continuity for each hand, the signals were low passed filtered at 7Hz and the marker velocity was calculated by finding the absolute difference in amplitude for consecutive time points. Calculating velocities as opposed to displacements removed any spatial drifts present in the 3-d position motion capture signals occurring due to subjects changing the vertical position of their wrists during the trial, while retaining the characteristics of the motion. As there were amplitude and timing differences between the tapping fingers and it was desired to have a single kinematic regressor for each tapping hand, principal component analysis (PCA) was performed to the velocity profiles of the included distal markers and the first principal component was used to make the

corresponding kinematic regressors. Next, the data was down-sampled from 120 Hz to 25 Hz to match the sampling rate of the fNIRS system. Finally, the processed motion tracking data was convolved with the HRF used previously in the standard GLM analysis.

Kinematic regressors were also created using EMG signals. The EMG signals were all continuous in time and therefore creation of the regressors was more straightforward. The signal from the finger extensor muscle from each arm was used to make the corresponding tapping and mirror hand regressors. After filtering as described in the signal processing section, the signal was down sampled from 1000 Hz to 25 Hz to match the fNIRS sampling rate, and then convolved with the same HRF as used previously.

The final step in creating the kinematic regressors for both motion tracking and EMG was to remove any tapping blocks that were removed during the processing of fNIRS data due to motion artifacts so that the kinematic and fNIRS data streams were synchronized.

2.5.3 Determination of the Maximum Number of Independent Components Supported by the FNIRS Data Sets

All independent component analysis in this study was performed with the FastICA algorithm provided online by researchers at the University of Helsinki [34]. This algorithm receives as input the data on which the ICA is to be performed, the number of ICs to be found, and other optional parameters. For the optional parameters the skew option was chosen for nonlinearity, 10000 was chosen for the maximum number of iterations, and all other options were not specified, therefore the default parameters were used. The FastICA algorithm was initially run with the ΔHbO time series for each pixel as the input data starting with 40 ICs. 40 ICs proved to be too many for all data sets as the algorithm failed to converge consistently with this many ICs. To determine the maximum

possible number of ICs, the number of ICs was reduced and the algorithm was run again. This process was repeated until the algorithm converged three times for the number of components chosen. This number was not consistent between data sets and the number of components found ranged from 20-35. The identified ICs and the mixing matrix A (see equation (1.5)) created by each one of these components were saved to be used in the next step of the analysis.

2.5.4 Determination of Independent Components

The first step the FastICA algorithm takes is to choose a random initial value for the weighting vector *w*, which is one of the rows in the separating matrix *W* (see equation (1.6)). Because this initial value is chosen randomly the ICs found in one run of the FastICA algorithm may not be the same ones found in a different run as different initial values may converge to different solutions. This poses a problem as different runs may produce different results, and therefore different activation images. Despite this inconsistency, some components are always found by the algorithm, so in order to obtain consistent results only these ICs were used in the analysis.

To determine which ICs were found consistently an initial run of the FastICA algorithm was performed and the ICs were saved (see section 2.5.3). Then the FastICA algorithm was run 30 times on the same data set. For each iteration a correlation coefficient was found between each IC from the current iteration and all the saved ICs using the MATLAB function corrcoef. The correlation coefficients were stored in a square matrix with dimensions equal to the number of ICs used for the particular data set. In this matrix, rows represented the saved ICs and columns represented the ICs from the current iteration. By finding the maximum absolute value in each row, all the saved independent components were matched to one of the components in the current run. To

help illustrate the process, an abbreviated sample of this matrix for one iteration is shown in Figure 2-4.

Current Components

Saved Components

	1	2	3
1	0.016553	0.999856	4.26E-05
2	-0.05364	0.000842	0.99854
3	0.988005	0.001197	-0.00187

Figure 2-4 Abbreviated correlation coefficient matrix for one run of the ICA algorithm

In Figure 2-4, the second component from the current run would be matched with the first saved component because 0.9998 is the maximum correlation coefficient in the row. Similarly, current components 3 and 1 would be matched with saved components 2 and 3, respectively. It should be noted that no saved component will ever be highly correlated with more than one current component because all independent components within the same run are by definition uncorrelated. The same is also true in the opposite direction where no current component will be highly correlated with multiple saved components.

A matrix was created to save the maximum correlation coefficient values found for each saved IC on each run of the ICA algorithm. Each row in this matrix contained the maximum correlation coefficients found for one of the saved ICs. After the 30 runs, each saved IC had 30 matched maximum correlation coefficients in its row. Those that were found consistently would have a match in all runs of the algorithm and therefore all the

matched correlation coefficients would be high. Therefore the average of the 30 correlation coefficients was found for each saved IC, and those with an average 0.9 or higher were considered to be found consistently. The saved ICs with an average correlation coefficient value of less than 0.9 were discarded because they were not found in some of the runs of the ICA algorithm.

2.5.5 Regression of Kinematic Independent Components with FNIRS Data

During each of the 30 runs of the FastICA algorithm a GLM analysis was performed on the independent components as given in equation 2-2.

$$\boldsymbol{Y} = X_0\beta_0 + X_1\beta_1 + X_2\beta_2 + X_1X_2\beta_3 + \boldsymbol{\epsilon} \tag{2.2}$$

In equation 2-2 *Y* represents a matrix containing the independent components of fNIRS data form each image pixel, X_1 and X_2 represent the motion tracking or EMG regressors for the tapping and non-tapping hand respectively, β_1, β_2, and β_3 are the corresponding scaling factor model estimates, and X_0 and ε are the DC and error terms as in equation 2.1. The X_1X_2 term was included as a statistical interaction term to reduce the amount of cross-talk in the model as the tapping and mirror hand motion regressors are usually correlated to varying degrees. To determine if either of the regressors explained a statistically significant amount of the variance in any of the independent components, t-values were calculated using equation 2-3.

$$t = \frac{c'\boldsymbol{\beta}}{\sqrt{Var(\boldsymbol{\epsilon})c'(\boldsymbol{X}'\boldsymbol{X})^{-1}c}} \tag{2.3}$$

In equation 2.3 all terms were introduced in equation 2.2 except for *c*, which represents a contrast vector. Modification of this vector allows different null hypotheses to be tested. In this work, to determine if activation was significantly above baseline a contrast multiplying β_0 by -1 and the β of interest by 1 was used while all other β values

were multiplied by 0. For example, to test if the tapping hand regressor X_1 was significant, a contrast vector of [-1 1 0 0] was used in equation 2.3.

For each of the 30 runs t-values were calculated for the tapping hand regressor and mirror hand regressor for each independent component. Since each component was matched to a saved component using the method described in the previous section, the t-values could also be matched to a saved component. These t-values were saved for each run resulting in a total of 60 t-values for each saved independent component, 30 for the tapping hand regressor and 30 for the mirror hand regressor.

2.5.6 Selection of Independent Components for Image Creation

In order to create an image for each motion regressor only certain ICs were chosen from those saved after the initial run of the ICA algorithm (see section 2.5.3). First, the components with average matching correlation coefficients less than 0.9 were excluded because they were not found consistently by the algorithm. (see section 2.5.4). It was then necessary to determine if either motion regressor explained a significant amount of the variability in the remaining ICs. With the application of the Bonferroni's correction it was determined that a t-value of greater than 3.5 or less than -3.5, as calculated with equation 2.3, indicated that a regressor did explain a significant amount of the IC. Since each saved IC had 30 t-values for each motion regressor (see section 2.5.4), a one sample t-test was performed on each set of t-values to test the null hypothesis that the absolute value of the t-value for a component was less than 3.5. A right sided t-test was performed on the absolute values of the t-values with $\alpha = 0.05$ using the ttest function in MATLAB. If the function returned 1, then the null hypothesis was rejected and it was concluded that the regressor being tested did explain a significant amount of the variance in the IC.

After performing the t-tests on the t-values for both motion regressors and for all ICs, each regressor either did or did not significantly explain each IC. ICs not significantly explained by either regressor were simply discarded at this step. ICs which were explained by both regressors were also excluded because images made with these ICs would be correlated with both tapping and mirror motions. ICs that were significantly explained by only one regressor were kept, with one group of ICs explained only by the tapping hand regressor and one explained only by the mirror hand regressor. These ICs were used in the next step of the analysis.

2.5.7 Creation of Activation Images

After selecting a group of ICs for each regressor, activation images were created using only these components. However, before making the images a correction needed to be made to the mixing matrix A (see equation 1.5). It was observed that when making an image out of a single independent component some pixels in the image would match the sign of the corresponding pixel in the standard boxcar image, but others would not. This occurs because the ICA analysis takes the other ICs into account when creating the mixing matrix so that all the ICs add to original signals. Since activation images using the GLM/ICA method are created using only a few components, some activation areas may differ in sign from the final image. In order to correct this discrepancy, the ΔHbO time series were reconstructed for each component using equation 2.4.

$$\boldsymbol{Y_{ICA} = A * C * x} \tag{2.4}$$

In equation 2.4, Y_{ICA} is the matrix containing the ΔHbO time series for each pixel, A is the saved mixing matrix, x represents the saved ICs, and C is a square matrix with a 1 in the diagonal position corresponding to the selected saved component. Elsewhere, the matrix C is populated with zeroes. The ΔHbO time series acquired in equation 2.4 were then used in a GLM analysis as given in equation 2.5.

$$\boldsymbol{Y_{ICA}} = X_0\beta_0 + X_1\beta_1 + \boldsymbol{\epsilon} \quad (2.5)$$

In equation 2.5 X_1 represents either the tapping hand or mirror hand motion regressor, depending on which group the component being analyzed belonged to. Y_{ICA} was introduced in equation 2.4, and all other variables were introduced in equation 2.2. The β_1 values obtained from equation 2.5 were compared to their corresponding ΔHbO values from the standard GLM boxcar analysis on a pixel by pixel basis. In cases where the β_1 and ΔHbO values differed in sign, the appropriate weight in the mixing matrix A was multiplied by -1. After this modification, the pixels in the final activation images had the correct sign.

After correcting the mixing matrix, two sets of ΔHbO time series were reconstructed using equation 2.4, one set for the tapping hand motion and one for the mirror and motion. For each set, the *C* matrix was modified to have a 1 on the diagonal for each component included in its respective group. A GLM was performed two more times, once for the tapping hand ΔHbO time series and once for the mirror hand ΔHbO time series, using equation 2.5 with the corresponding motion regressor. However, before performing the GLM analysis both motion regressors were normalized by dividing them by their maximum values. This normalization allowed the β values computed by the GLM analyses to approximate the magnitude of the ΔHbO. A β value was found for each image pixel using the GLM analysis, and since these values approximated ΔHbO, they were used to make the activation images. One image was created using the β values from the GLM analysis using the tapping hand regressor and one was created the β values from the GLM analysis using the mirror hand regressor, resulting in a ΔHbO activation image for each motion type. Figure 2-5 is included below and gives a detailed flow chart of all the steps previously described.

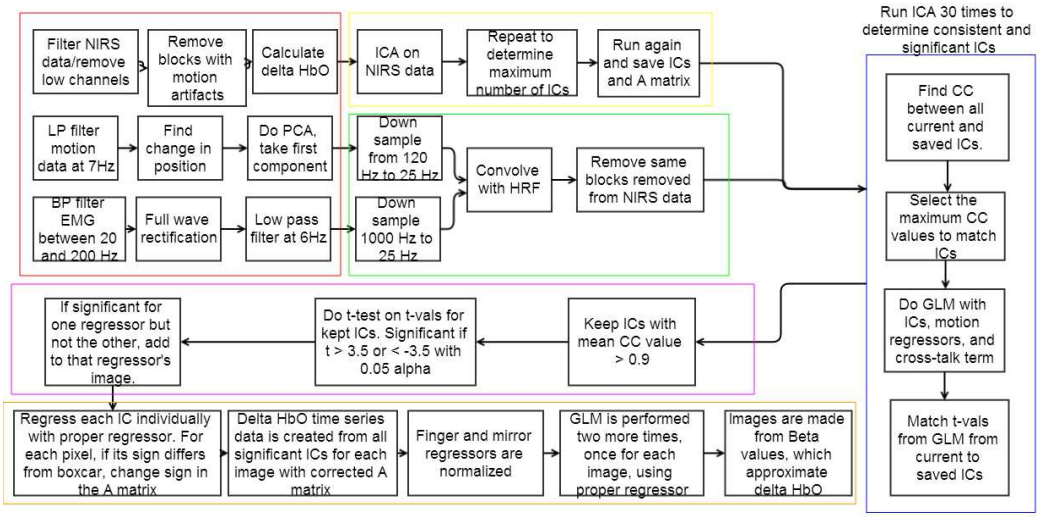

Figure 2-5 Detailed Overview of the GLM/ICA method

Chapter 3

Results and Discussion

3.1 Eligible Data Sets for the GLM/ICA Method

Unfortunately, many data sets had to be excluded from analysis with the GLM/ICA method due to a variety of reasons including motion artifacts in the fNIRS data, incomplete motion capture data due to target occlusions, and the absence of mirror motions from many of the recruited children with CP. Table 3-1 gives a summary of collected data, and indicates why some data sets were excluded. The green cells of Table 3-1 are data sets that fit the criteria for the GLM/ICA method and therefore were analyzed. The yellow cells indicate that no mirror motions were present. In these cases the GLM/ICA method cannot be applied. The red cells are unusable data and indicate why this is the case. The most frequent reason was motion artifacts except for Subject 5 who was non-compliant because he did not follow the protocol well enough to provide reliable data in any trials. Another reason for the incomplete data set collection was that Subject 4 did not return for his third visit. All in all, there were a total of 46 data sets to begin with. Irrespective of any presence of mirror motions the overall fNIRS success rate when excluding data sets with motion artifacts was roughly 70%. In 23 of these data sets the subjects exhibited no mirror motions and in 15 cases the data was not usable leaving only 8 eligible data sets, which is relatively low compared to the total. Despite the small eligibility rate, it will be shown that the proposed GLM/ICA method does provide useful information about how mirror motions are mapped onto the sensorimotor cortex in some cases, and these results are discussed in the next sections.

Table 3-1 Summary of data sets from all subjects

Subject	Tapping Hand	Visit 1	Visit 2	Visit 3
1	Right	No mirror motions	No mirror motions	No mirror motions
	Left	No mirror motions	No mirror motions	No mirror motions
2	Right	Motion artifacts	Motion artifacts	Data analyzed
	Left	Motion artifacts	Motion artifacts	No mirror motions
3	Right	Motion artifacts	Data analyzed	No mirror motions
	Left	Motion artifacts	Data analyzed	Motion artifacts
4	Right	Data analyzed	No mirror motions	No data
	Left	No mirror motions	No mirror motions	No data
5	Right	Non-compliant	Non-compliant	Non-compliant
	Left	Non-compliant	Non-compliant	Non-compliant
6	Right	No mirror motions	No mirror motions	No mirror motions
	Left	No mirror motions	No mirror motions	No mirror motions
7	Right	No mirror motions	No mirror motions	No mirror motions
	Left	No mirror motions	No mirror motions	No mirror motions
8	Right	Data analyzed	Data analyzed	Motion artifacts
	Left	Motion artifacts	Data analyzed	Data analyzed

.

3.2 Separation of Brain Activation Areas from Intended and Unintended Motions Using Motion Tracking

3.2.1 Subject 3 Left Hand Tapping Visit 2

The GLM/ICA analysis with subject-specific kinematic regressors was first applied to Subject 3 who was classified as MACS 2 and had impaired function of the left hand. Subject 3 was an interesting case because an area of his cerebral cortex to the right of the brain midline (including parts of the visual and sensorimotor cortex) was surgically removed due to seizures that did not respond to other treatments. This caused many of his brain's left side functions to shift to the right, including a move of his left sensorimotor area towards the brain center. Due to this surgery, some abnormal activation patterns were observed that will be discussed further in this section.

Figure 3-1a and Figure 3-1b show the vertical motion from the active (left) and resting (right) hand, respectively for Subject 3's left hand finger tapping task. Figure 3-1e shows the fNIRS image created using the standard boxcar regressor with the GLM.

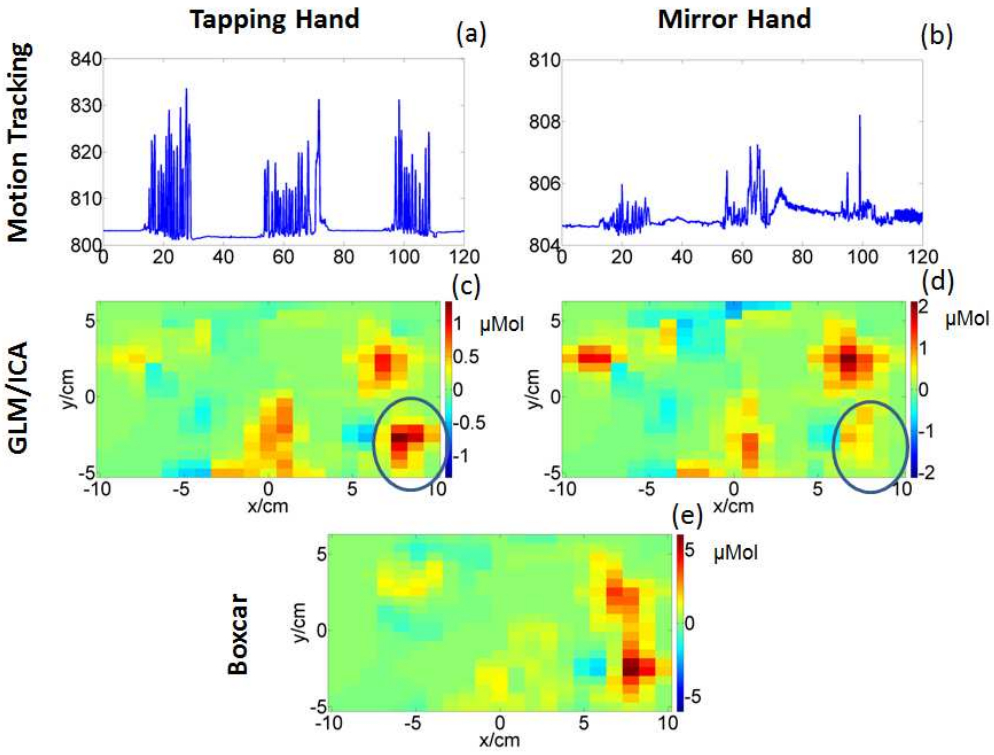

Figure 3-1 Comparison of activation images made with GLM/ICA method and boxcar regressor for Subject 3's left hand tapping: (a) Vertical position of nail target from active (left) hand, (b) Vertical position of nail target from resting (right) hand, (c) Image created using GLM/ICA method for active (left) hand, (d) Image created using GLM/ICA method for resting (right) hand, (e) Image made using boxcar regressor.

As expected there is significant contralateral motor and premotor activation seen on the right side of Figure 3-1e. However, the standard technique is limited as it does not take into account aberrant motions such as the mirror motions present in Figure 3-1b. The GLM/ICA method was applied in an attempt to address this shortcoming by attributing different activations areas to the intended or unintended motions by incorporating motion data into the fNIRS image formation process. Figure 3-1c and Figure 3-1d show the images created using the GLM/ICA method for the tapping (left)

hand and mirror (right) hand, respectively. Interestingly, the tapping hand image shows strong contralateral motor activation, while the mirror hand image shows relatively weak activation in the same area as indicated by the circles in Figure 3-1c and Figure 3-1d. This suggests the contralateral motor activation can be attributed to the tapping hand, as would be expected, and therefore supports the validity of the GLM/ICA method.

Also of interest are the premotor areas. Figure 3-1c-e all show bilateral premotor activation, with higher activation on the contralateral side. This indicates that the method is unable to attribute premotor activation to just one motion type. It is possible that both motions do in fact contribute to this activation, in which case the method would obviously not be able to separate the motions especially since the sensorimotor function of both hemispheres is largely mapped into a single hemisphere for this patient. This explanation is more likely in children with cerebral palsy that typically exhibit a higher degree of bilaterality in their sensorimotor activation patterns[45]. However, it is also possible that motion from only one hand caused the activation in each area, and the method was unable to determine which one was responsible. This latter possibility could occur because the intended and mirror motions are typically correlated, and therefore a complete separation of activation areas cannot be achieved. Similar to the premotor areas, the midbrain areas show activation in all three images and cannot be singularly attributed to either hand.

3.2.2 Subject 3 Right Hand Tapping Visit 2

The GLM/ICA method was also applied to Subject 3's right hand tapping task from the same visit. Figure 3-2a and Figure 3-2b show the images created using the GLM/ICA method for the tapping (right) and resting (left) hands, respectively, and Figure 3-2c shows the image created using the standard boxcar regressor with the GLM. Figure 3-2a-c show an atypical activation pattern for right hand motion as there appears to be no

contralateral motor area activation. However, as mentioned earlier this subject had surgery, which effectively shifted his left motor area towards the brain's center. Therefore, the midline activation seen in Figure 3-2a-c is likely related to maladaptive mapping of left motor area functions.

Figure 3-2a and Figure 3-2b show that one area of activation is present in the tapping hand image but absent from the mirror hand image as indicated by the circles, but are otherwise similar. These results are similar to those obtained for Subject 3's left hand tapping, but the interpretation is not as obvious. Figure 3-1c indicates that the left hand maps to the right motor area as expected, but it seems that Figure 3-1a suggests the right hand is also mapped to the right motor area as the circled area is typically associated with this region. However, comparison of Figure 3-1c and Figure 3-2a reveal that these activation areas are adjacent, but not the same. The right hand activation circled in Figure 3-2a is higher and farther to the left relative to the left hand activation circled in Figure 3-1c. These figures are printed next to each other in Figure 3-3 with the areas of interest indicated by arrows and circles. This mapping would certainly be abnormal for a typical child, but because Subject 3 has cerebral palsy and had part of his cortex removed, a typical activation patter should not be expected. In fact, even the boxcar images of Figure 3-1e and Figure 3-2c show adjacent but distinctly different activation regions in the middle to lower right side of the images. Therefore, it seems that the GLM/ICA method does correctly map the right hand to the area circled in Figure 3-2a.

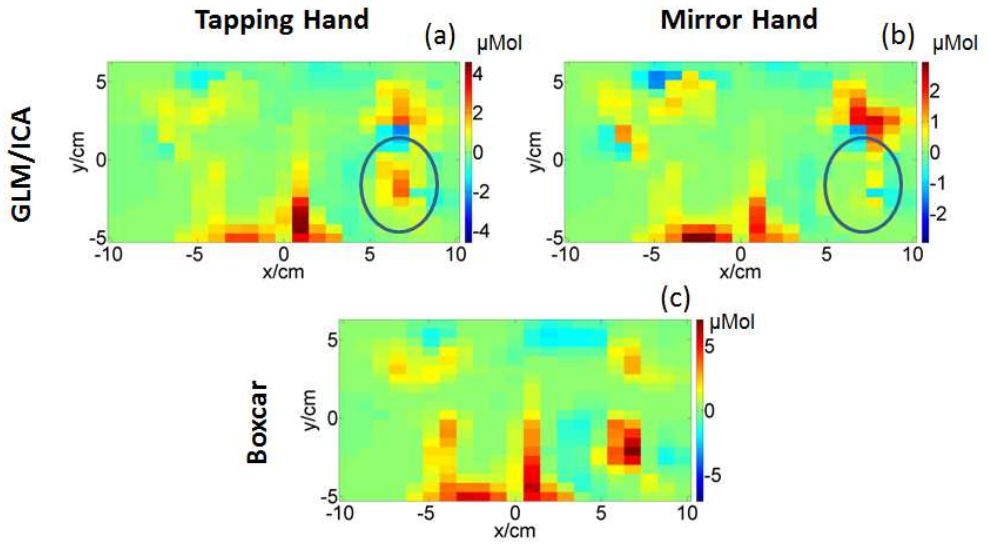

Figure 3-2 Comparison of activation images made with GLM/ICA method and boxcar regressor for Subject 3's right hand tapping: (a) Image created using GLM/ICA method for active (right) hand, (b) Image created using GLM/ICA method for resting (left) hand, (c) Image made using boxcar regressor

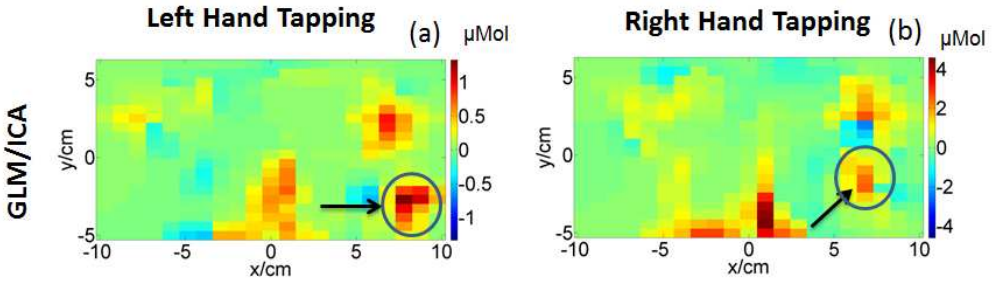

Figure 3-3 Comparison of tapping hand GLM/ICA images for Subject 3's left and right hand tapping: (a) GLM/ICA image for left hand during left hand tapping trial (b) GLM/ICA image for right hand during right hand tapping trial

Aside from this region, the method fails to attribute activation areas to only one motion. Similar to the results from the left hand, Figure 3-2a-c all show bilateral premotor activation. Since this activation is seen in both left and right hand tapping, it is possible that both hands contribute to this premotor activation, but not certain. There is also significant midline activation in Figure 3-2a-c, and again the method does not reveal which motion is responsible. However, since there is relatively weak activation in this area during left hand tapping (Figure 3-1e), it is likely that the right hand motion was mostly responsible for this activation. The appearance of strong midline activation even in the mirror image is likely due to the correlation between the tapping and mirror kinematic regressors used in this analysis.

3.2.3 Subject 2 Right Hand Tapping Visit 3

The GLM/ICA method was next applied to Subject 2, who was MACS 2 and had impaired function of the right hand. Figure 3-4a and Figure 3-4b show the results for the tapping (right) hand and resting (left) hand, respectively, Figure 3-4c shows the standard boxcar image for right hand tapping, and Figure 3-4d shows the boxcar image from Subject 2's left hand tapping task from the same visit. Figure 3-4d is included here because Subject 2 did not exhibit mirror motions when tapping with his left hand, so the GLM/ICA method could not be applied.

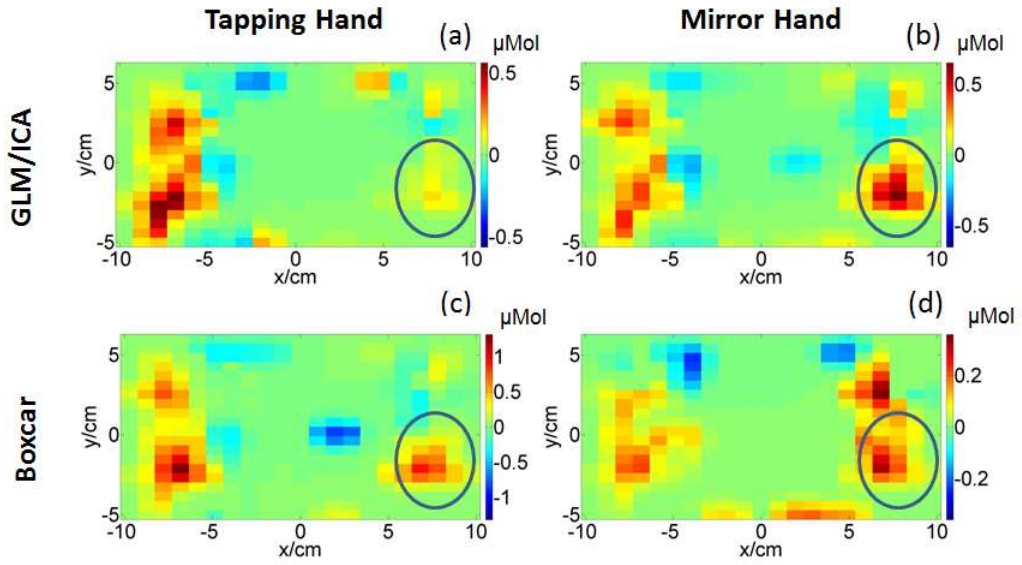

Figure 3-4 Comparison of activation images made with GLM/ICA method and boxcar regressor for Subject 2's right hand tapping: (a) Image created using GLM/ICA method for active (right) hand, (b) Image created using GLM/ICA method for resting (left) hand, (c) Image made using boxcar regressor for right hand tapping, (d) Image made using boxcar regressor for left hand tapping from same visit.

Figure 3-4c shows bilateral motor activation and contralateral premotor activation relative to the right hand motion. Comparing Figure 3-4a to Figure 3-4c, it is apparent that motor activation is now contralateral, with only weak ipsilateral motor activation, as would be expected. In contrast, Figure 3-4b, which shows activation correlated to the mirror (left) hand motions retains the activation located in the right motor area indicated by the circle. These results suggest that the ipsilateral motor activation seen in the standard boxcar image (Figure 3-4c, circled area) is actually due to left hand mirror motion and not right hand motion. This conclusion is further supported by the boxcar image from the left hand tapping task (Figure 3-4d), which like Figure 3-4b, shows strong activation in the right motor area. Based on this conclusion, the GLM/ICA method provided an activation

image for the active hand (Figure 3-4a) that more accurately represented the brain areas responsible for the motion by removing the ipsilateral motor activation attributed to left hand.

Despite these positive results, the method was not able to provide complete separation. Figure 3-4a-c all show significant activity in the left motor and premotor areas. As with Subject 3, it may be the case that only one motion caused activation in these areas, or they could both be responsible. Here the latter case seems more likely, as left motor and premotor activation is seen during left hand tapping (Figure 3-4d) with no right hand mirror motions present. If both motions did contribute to these areas, then the GLM/ICA method did provide correct results as activation is seen in Figure 3-4a and Figure 3-4b, but this cannot be determined with certainty because intentional and mirror signals are not completely uncorrelated.

3.2.4 Subject 8 Right Hand Tapping Visit 2

Subject 8 was classified as MACS 2, with impairment in the right hand. He exhibited mirror motions during left and right hand tapping, so the GLM/ICA method was applied for each case. Figure 3-5a and Figure 3-5b show the results for the tapping (right) hand and resting (left) hand, respectively and Figure 3-5c shows the standard boxcar image. The boxcar image shows bilateral motor activation and ipsilateral premotor activation. From this image alone, one would assume the right hand motion was responsible for all this activity. However, the images created with GLM/ICA method suggest this is not the case. Notice the left motor area in Figure 3-5a-c indicated by the blue circles. This activation area is strong in the tapping (right) hand image (Figure 3-5a), but almost nonexistent in the mirror image (Figure 3-5b), indicating that right hand motion was responsible for this activation. The opposite is true for the right motor area, indicated by the red circles in Figure 3-5a-c. There is significant activity in the right motor area in

the mirror (left) hand image (Figure 3-5b), but not the tapping (right) hand image (Figure 3-5a). In this case, the GLM/ICA method is able to attribute the left motor activation seen in Figure 3-5c to right hand motions, and activation in the right motor area to left hand motion, as would be expected. However, as in the previous cases the method was unable to attribute the premotor area activation to only one motion though more contralateral premotor activation is seen in the mirror hand image as indicated by the gray circles in Figure 3-5a and Figure 3-5b.

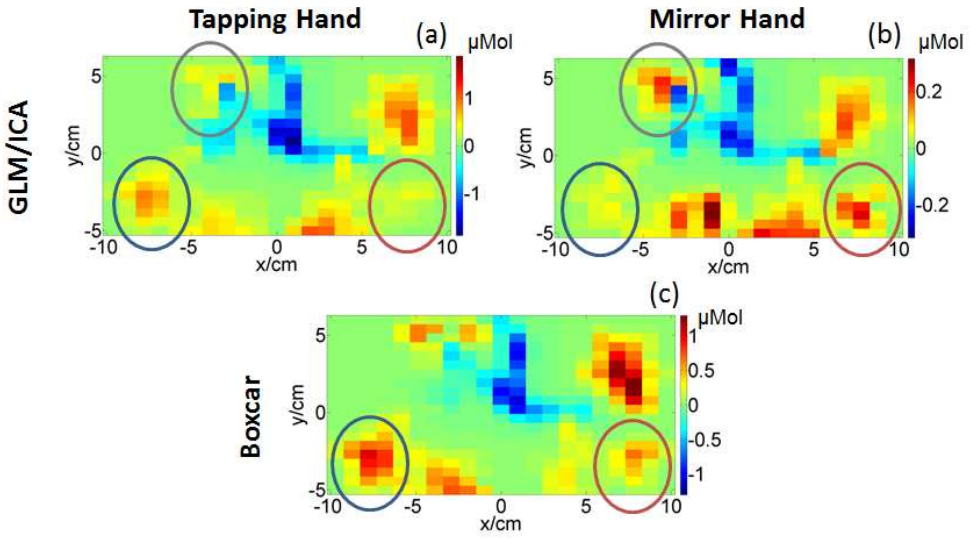

Figure 3-5 Comparison of activation images made with GLM/ICA method and boxcar regressor for Subject 8's right hand tapping: (a) Image created using GLM/ICA method for active (right) hand, (b) Image created using GLM/ICA method for resting (left) hand, (c) Image made using boxcar regressor.

3.2.5 Subject 8 Left Hand Tapping Visit 2

Subject 8 also showed mirror motions during his left hand tapping at the same visit, so the GLM/ICA method was applied. However, for left hand tapping the GLM/ICA

did not provide meaningful results. Figure 3-6a-c show the activation images for the tapping, mirror, and boxcar images, respectively. Notice that Figure 3-6a and Figure 3-6b look nearly identical, except for minor differences in the right premotor area and midline areas. These slight differences are small compared to the differences in the previously discussed cases, so effectively all the activation areas present in the tapping image (Figure 3-6a) are also present in the mirror image (Figure 3-6b) with the same relative amplitude, thus no further information is gained with GLM/ICA method.

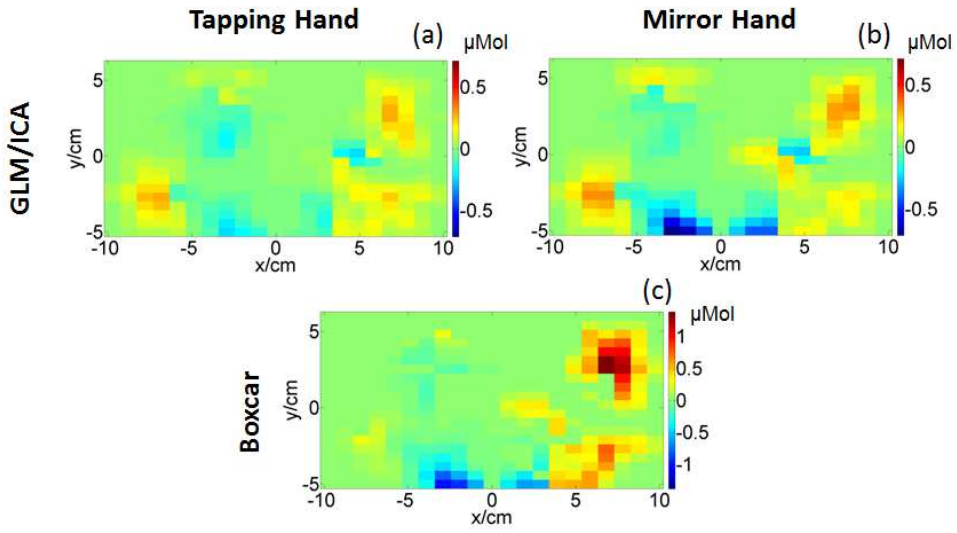

Figure 3-6 Comparison of activation images made with GLM/ICA method and boxcar regressor for Subject 8's left hand tapping: (a) Image created using GLM/ICA method for active (left) hand, (b) Image created using GLM/ICA method for resting (right) hand, (c) Image made using boxcar regressor.

The obvious question is why did the method work in the previous cases and not this one? The answer is the kinematic regressors created from the tapping hand and mirror hand motions are too highly correlated. In this particular case, the subject had much higher amplitude mirror motions (20-80 mm) while tapping with his unaffected (left)

hand, with motion occurring in the mirror (right) hand on nearly every tap. While tapping with his right hand, mirror motions in the left hand were of much lower amplitude (2-12mm), and did not occur on every tap made by the tapping hand. This resulted in a higher correlation between the motions for the unaffected (left) hand tapping trial, and therefore the motion regressors which were highly correlated.

Table 3-2 gives the correlation coefficients between the tapping and mirror kinematic regressors for each case, including two additional cases with negative results. Notice that the correlation coefficient values for the negative result cases are the three highest in Table 3-2. As the correlation coefficient increases, the components selected for the finger and mirror images tend to produce similar images, which provide little to no separation of the motions. The results of this study suggest that correlation coefficient values above 0.79 do not produce meaningful results. However, since a value of 0.78 did produce meaningful results there is likely a range of values in which the method may or may not provide useful information. More tests would be needed to confirm this, and establish a range of values. The high correlation between motion regressors is one limitation of the GLM/ICA method as it excludes trials with high correlation between tapping and mirror motions that otherwise might benefit from the method's application.

Table 3-2 Correlation coefficients between tapping and mirror kinematic regressors for different trials.

Trial	Correlation Coefficient	Positive Result?
Subject 3 LH V2	0.59	Yes
Subject 3 RH V2	0.78	Yes
Subject 2 RH V3	0.62	Yes
Subject 8 RH V2	0.72	Yes
Subject 8 LH V2	0.93	No
Subject 8 RH V1	0.79	No
Subject 8 LH V3	0.92	No

3.3 Separation of Brain Activation Areas from Intended and Unintended Motions Using EMG

3.3.1 Subject 4 Right Hand Tapping

The GLM/ICA method was also applied to Subject 4, who was classified as MACS 1 and had impairment in his right hand. Subject 4 presented a unique case because he did not have any visible mirror motions, however there was muscle activity recorded with the EMG in his left extensor, which indicates he was pushing against the table with his mirror hand. Since mirror motions were not present in the motion tracking data, the kinematic regressors were instead made from the EMG signals. Figure 3-7a-c shows the tapping, mirror, and boxcar activation images, respectively.

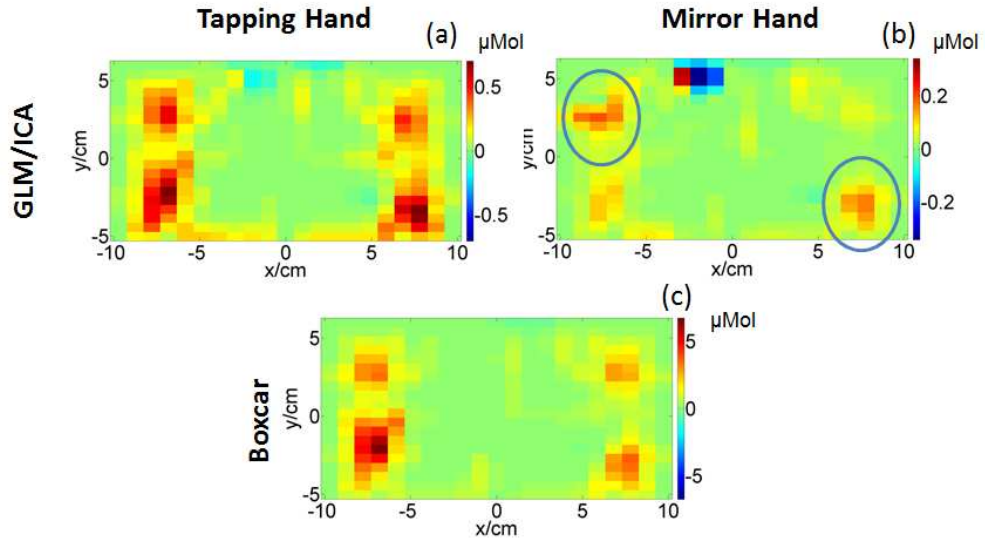

Figure 3-7 Comparison of activation images made with GLM/ICA method and boxcar regressor for Subject 4's right hand tapping: (a) Image created using GLM/ICA method for active (right) hand, (b) Image created using GLM/ICA method for resting (left) hand, (c) Image made using boxcar regressor.

Figure 3-7c shows bilateral activation in the motor and premotor areas, with the highest amplitude activation in the contralateral motor area. Comparing this to Figure 3-7a, it is apparent that the tapping image also shows bilateral activation in the motor and premotor areas, thus the right hand motion was correlated with all activation areas. On the other hand, Figure 3-7b shows relatively high activation in the right motor area, which is responsible for left hand muscle activity, and in the left premotor area. In addition, there is activation in the left motor and right premotor areas, but it is weak relative to the other areas. These results suggest that the left (mirror) hand muscle activity likely contributed most to the right motor area and left premotor area. Again, the GLM/ICA method shows some utility, as the information regarding mirror hand activation is not obtainable using the standard GLM with the boxcar regressor.

3.4 Motion Tracking Versus EMG for Kinematic Regressor Creation

An obvious question is that if regressors made from EMG data produce successful results, why use motion capture data instead? EMG measurements have several advantages over motion capture measurements. They are less expensive, require less room and set-up time, and data processing is less taxing. However, as Table 3-3 shows, the regressors made using EMG data are typically more correlated than those made with motion capture data. As discussed previously, higher correlation coefficients between the tapping and mirror hand regressors produce less meaningful results. For this reason motion capture data is superior to EMG data when using the GLM/ICA model. Note that no motion tracking correlation coefficient is given for Subject 4’s because he had no visible motions. This unique case produced EMG regressors with a very low correlation coefficient, which is not typical for these regressors.

Table 3-3 Comparison of correlation coefficients for motion tracking regressors and EMG regressors

	Motion Tracking CC	EMG CC
Subject 3 LH V2	0.59	0.72
Subject 3 RH V2	0.78	0.82
Subject 2 RH V3	0.62	0.88
Subject 8 RH V2	0.72	0.95
Subject 8 LH V2	0.93	0.96
Subject 4 RH V1	-	0.08

3.5 Overall Trends

Some overall trends are apparent in the results produced by the GLM/ICA method. First, the method does not attribute premotor activation to only one motion in any of the cases where motion tracking data was used to make the regressor. As discussed earlier, it is possible that both motions do contribute to the premotor areas, in which case the method correctly identifies this. On the other hand, since the motions are at least somewhat correlated in all cases, the method may attribute premotor activation to both motions when only one is responsible. Either of the explanations may be true for each individual case, and the GLM/ICA method does not provide the means to know which is true.

The method provided useful information in several cases, but not in the same way. In two cases, for Subject 2's right hand tapping and Subject 8's right hand tapping, the method removed an activation area from the tapping image that was present in the standard boxcar image. In both cases the activation area removed was the ipsilateral motor area. This area did show activation in the mirror hand images, which suggests that the activity seen in the boxcar image was in fact due to mirror hand motions. In these two cases the GLM/ICA was able to provide an image for the tapping hand that better represented activation due only to this motion as compared to the standard method and

therefore gave superior results. For the other three successful cases, two with motion tracking and one with EMG, activation areas were removed from the mirror hand image rather than the tapping image. Although this does not result in a tapping image with some removal of mirror motion activation as in the other two cases, it does provide some useful information about the origin of each activation area. Since activation areas are present in the tapping and boxcar images but not in the mirror images, this activation can be attributed to the tapping hand alone. In other areas, the motion or motions responsible for activation are still in question due to the high correlation of brain signals. This still provides an advantage over the standard boxcar technique, where the origin of all activation areas is in question due to the fact that mirror hand motions are not taken into consideration.

3.6 Limitations

Although the method did prove to be useful in a few situations, it does have several limitations. One major limitation is the presence of motion artifacts in the data. FNIRS does provide better resistance to these artifacts than other functional neuroimaging techniques such as fMRI, but it is not completely immune, especially when working with children. Some children had significant head motions throughout the trials, and these data sets had to be excluded due to motion artifacts. Another limitation was the reliability of the motion capture data. Some children became restless during the inactive periods and moved their hands out of the field of view of the cameras. Other children moved in ways that caused some targets to be occluded during motion. These issues became worse after the first two trials when the study was moved to a smaller with room with less space for the cameras (see methods section). Fortunately in this study these problems were only severe in cases where the trial had to be excluded for other reasons,

but if used in future studies the motion tracking system's unreliability could prove to be problematic.

Another limitation is that not all children with cerebral palsy exhibit mirror motions during the hand tapping task. In these cases where only one motion is present the GLM/ICA method obviously cannot be used since its purpose is to attribute activation areas to different motions. In children who do have mirror motions, these are typically correlated to some degree. When these motions are highly correlated (CC >= 0.79) the kinematic regressors created using the marker velocity data are so similar that they produce nearly identical tapping and mirror images resulting in no useful information.

Chapter 4

Conclusion

Current fNIRS image analysis techniques assume that a subject has followed a given activation protocol correctly, which is not necessarily the case and especially so in subjects with motor deficits. The goal of this work was to help address this current gap in the field by studying how cortical activation patterns mapped by fNIRS during a unimanual hand tapping task are affected by the presence of unintended, or mirror, motions of the non-tapping hand in children with CP. The hypothesis of this work was that concurrent recording of finger motions and arm muscle activity for both tapping and non-tapping hands would help separate the contributions of tapping and mirror motions to fNIRS images. To test this hypothesis a new fNIRS image analysis method, that we call GLM/ICA, was developed and applied to data acquired from eight children with CP. By simultaneously acquiring fNIRS signals from the sensorimotor cortex, EMG signals from the major arm muscles, and motion capture data from markers placed on the fingers it was possible to include information about the subject's motion intp the fNIRS data analysis. Two motion regressors were created using the motion capture or EMG data, one for intended and one for unintended motions. Also, ICA was applied to the ΔHbO time series to isolate different activation signals present in the data. A GLM analysis was performed on the independent components using the two motion regressors, and two activation images were made using the results. An image for the intended hand motion was created using the independent components which were significantly explained only by the intended motion regressor, and an image for the unintended motions was made in the same way.

A total of 46 measurements were performed on the eight children with CP, but only eight of these measurements were eligible for use with the GLM/ICA method as several of the children did not have mirror motions and motion artifacts were present in some of the fNIRS signals. The method provided meaningful results for five of the eight eligible data sets across four subjects, as the other three data sets were highly correlated. For Subject 3 motion capture data was used in the analysis and two data sets provided meaningful results. For the trial in which Subject 3 tapped with his affected (left) hand, an activation area located in the right primary motor cortex in the tapping hand and boxcar images was removed from the mirror hand image. This suggests that the intended tapping motions were primarily responsible for the activation in this area and therefore provides information not available using only the standard boxcar analysis. The method was also applied to his unaffected (right) hand tapping, and again an activation area present in the boxcar and tapping image was removed from the mirror image resulting in a similar conclusion.

The method was also applied to Subject 2's affected (right) hand tapping task using motion capture data. In this case activation in the right motor cortex that was present in the boxcar image was removed from the tapping hand but not the mirror image. Here the method was able to clean up the tapping hand image by removing an activation area that was actually due to the mirror hand motion, thus providing superior results to the standard boxcar analysis.

Similar results were obtained for Subjects 8's affected (right) hand tapping, again using motion capture data. The boxcar image for this task showed bilateral activation in the primary motor cortex. However, for the tapping (right) hand image, the activation in the right primary motor cortex was removed, while in the mirror (left) hand image the activation in the left primary motor cortex was removed. This suggests that the right hand

was responsible for the left motor activation and the left responsible for the right motor activation, which would be expected. Again the two images produces by the method provide more information than the boxcar image alone.

Finally, the method provided meaningful results for Subject 4's affected (right) hand tapping task, but using EMG signals instead of motion capture data because the subject pressed against the table with his mirror hand and therefore had no visible mirror motions. In this case bilateral motor and premotor activation was present in the tapping hand and boxcar images. However, the activation in the left motor and right premotor areas were largely removed in the mirror image indicating that the mirror (left) was primarily contributed to the activation in the right motor and left premotor areas. As before this information would not be available with only the boxcar image, so the method again proves to be valuable.

Despite these positive results, the method has several limitations. First, some activation areas are present in all three images. In these cases it cannot be determined if the activation is due to both motions or if only one motion is responsible and the method simply cannot determine this. Also, the method did not provide meaningful results for three of the eligible data sets because the motion regressors were too highly correlated. When this occurs the independent components selected for the two motions are too similar and therefore produce nearly identical activation images. Related to this limitation is the fact that motion regressors created with EMG signals produce inferior results compared to those made from motion capture data because EMG regressors are more correlated than their motion tracking counterparts.

Due to the limitations discussed above and the low number of cases relative to the total number of available data sets, the information gained from the GLM/ICA method is likely not worth the extra equipment and time required to use it, unless it is known

upfront that subjects have strong mirror motions. Therefore this work indicates that the GLM/ICA method would potentially be more applicable to more affected patients. If the method is used on a patient with strong unintended motions care should be taken to limit head motions by the subject to reduce the occurrence of motion artifacts in the fNIRS signals. Also, the placement of the motion capture cameras should be carefully considered to reduce the amount of occlusions and dropouts in the motion capture system. Because EMG signals provide more highly correlated results than motion capture data, it is recommended that they be used in any future studies using the GLM/ICA method only if other forms of kinetic data are not available.

References

1. Kalat, J.W., *Biological Psychology*. 11th ed. 2013, Mason, OH: Cengage Learning.
2. ; Available from: http://thebrain.mcgill.ca/flash/a/a_06/a_06_cr/a_06_cr_mou/a_06_cr_mou.html.
3. Brown, A. 2012; Available from: http://www.acbrown.com/neuro/Lectures/Motr/NrMotrPrmr.htm.
4. OpenStaxCollege. *Motor Responses*. June 28, 2013; Available from: http://cnx.org/content/m46574/latest/?collection=col11496/latest.
5. Oskoui, M., et al., *An update on the prevalence of cerebral palsy: a systematic review and meta-analysis.* Dev Med Child Neurol. **55**(6): p. 509-19.
6. Kulak, W. and W. Sobaniec, *Quantitative EEG analysis in children with hemiparetic cerebral palsy.* NeuroRehabilitation, 2005. **20**(2): p. 75-84.
7. Rosenbaum, P., et al., *A report: the definition and classification of cerebral palsy April 2006.* Dev Med Child Neurol Suppl, 2007. **109**: p. 8-14.
8. Eliasson, A.C., et al., *The Manual Ability Classification System (MACS) for children with cerebral palsy: scale development and evidence of validity and reliability.* Dev Med Child Neurol, 2006. **48**(7): p. 549-54.
9. Kuhtz-Buschbeck, J.P., et al., *Quantitative assessment of mirror movements in children and adolescents with hemiplegic cerebral palsy.* Dev Med Child Neurol, 2000. **42**(11): p. 728-36.
10. Huettel, S.A., Song, Allen W., McCarthy, Gregory, *Functional Magnetic Resonance Imaging*. 1st ed. 2004, Sunderland, MA: Sinauer Associates, Inc.

11. Pasley, B.N., Freeman, Ralph D., *Neurovascular coupling.* Scholarpedia, 2008. **3**(3): p. 5340.

12. Durduran, T., et al., *Diffuse optics for tissue monitoring and tomography.* Reports on Progress in Physics. **73**(7): p. 076701.

13. Chance, B., et al., *Phase measurement of light absorption and scatter in human tissue.* Review of Scientific Instruments, 1998. **69**(10): p. 3457-3481.

14. Phan, T.G. and A. Bullen, *Practical intravital two-photon microscopy for immunological research: faster, brighter, deeper.* Immunol Cell Biol. **88**(4): p. 438-44.

15. Scholkmann, F., et al., *A review on continuous wave functional near-infrared spectroscopy and imaging instrumentation and methodology.* Neuroimage. **85 Pt 1**: p. 6-27.

16. Zhao, H., et al., *Maps of optical differential pathlength factor of human adult forehead, somatosensory motor and occipital regions at multi-wavelengths in NIR.* Physics in Medicine and Biology, 2002. **47**(12): p. 2075.

17. Boas, D.A., A.M. Dale, and M.A. Franceschini, *Diffuse optical imaging of brain activation: approaches to optimizing image sensitivity, resolution, and accuracy.* Neuroimage, 2004. **23**: p. S275-S288.

18. Bunce, S.C., et al., *Functional near-infrared spectroscopy.* Engineering in Medicine and Biology Magazine, IEEE, 2006. **25**(4): p. 54-62.

19. Villringer, A. and B. Chance, *Non-invasive optical spectroscopy and imaging of human brain function.* Trends in neurosciences, 1997. **20**(10): p. 435-442.

20. Julien, C., *The enigma of Mayer waves: facts and models.* Cardiovascular research, 2006. **70**(1): p. 12-21.

21. Sato, T., et al., *Time courses of brain activation and their implications for function: a multichannel near-infrared spectroscopy study during finger tapping.* Neuroscience research, 2007. **58**(3): p. 297-304.

22. Furniss, M. *Motion Capture*. Available from: http://web.mit.edu/comm-forum/papers/furniss.html#fn4.

23. Hartley, R.Z., Andrew, *Multiple View Geometry in Computer Vision*. 2003, Cambridge: Cambridge University Press.

24. Silverthorn, D.U., *Human Physiology: An Integrated Approach*. 2007: Pearson/Benjamin Cummings.

25. Casellato, C., et al., *Simultaneous measurements of kinematics and fMRI: compatibility assessment and case report on recovery evaluation of one stroke patient.* J Neuroeng Rehabil. **7**: p. 49.

26. Holiga, S., et al., *Accounting for movement increases sensitivity in detecting brain activity in Parkinson's disease.* PLoS One. **7**(5): p. e36271.

27. MacIntosh, B.J., et al., *Improving functional magnetic resonance imaging motor studies through simultaneous electromyography recordings.* Human Brain Mapping, 2007. **28**(9): p. 835-845.

28. van Rootselaar, A.F., et al., *Simultaneous EMGâ€□functional MRI recordings can directly relate hyperkinetic movements to brain activity.* Human Brain Mapping, 2008. **29**(12): p. 1430-1441.

29. Lazar, N.A., *The Statistical Analysis of Functional MRI Data*. 2008: Springer-Verlag.

30. Molteni, E., et al., *GLM analysis of time resolved NIRS data of motor activation during different motor tasks.* Conf Proc IEEE Eng Med Biol Soc. **2013**: p. 1787-90.

31. Plichta, M.M., et al., *Model-based analysis of rapid event-related functional near-infrared spectroscopy (NIRS) data: a parametric validation study.* Neuroimage, 2007. **35**(2): p. 625-34.

32. Ye, J.C., et al., *NIRS-SPM: Statistical parametric mapping for near-infrared spectroscopy.* Neuroimage, 2009. **44**(2): p. 428-447.

33. Friston, K.J., et al., *Statistical parametric maps in functional imaging: A general linear approach.* Human Brain Mapping, 1994. **2**(4): p. 189-210.

34. Hyvarinen, A., *Fast and robust fixed-point algorithms for independent component analysis.* Neural Networks, IEEE Transactions on, 1999. **10**(3): p. 626-634.

35. Kohno, S., et al., *Removal of the skin blood flow artifact in functional near-infrared spectroscopic imaging data through independent component analysis.* Journal of Biomedical Optics, 2007. **12**(6): p. 062111-062111-9.

36. Santosa, H., et al., *Noise reduction in functional near-infrared spectroscopy signals by independent component analysis.* Review of Scientific Instruments. **84**(7): p. -.

37. Markham, J., et al., *Blind identification of evoked human brain activity with independent component analysis of optical data.* Human Brain Mapping, 2009. **30**(8): p. 2382-2392.

38. Zhang, H., et al., *Testâ€“retest assessment of independent component analysis-derived resting-state functional connectivity based on functional near-infrared spectroscopy.* Neuroimage. **55**(2): p. 607-615.

39. Klem, G.H., et al., *The ten-twenty electrode system of the International Federation. The International Federation of Clinical Neurophysiology.* Electroencephalogr Clin Neurophysiol Suppl, 1999. **52**: p. 3-6.

40. Tian, F., et al., *Enhanced functional brain imaging by using adaptive filtering and a depth compensation algorithm in diffuse optical tomography.* Medical Imaging, IEEE Transactions on. **30**(6): p. 1239-1251.

41. Huppert, T.J., et al., *HomER: a review of time-series analysis methods for near-infrared spectroscopy of the brain.* Applied Optics, 2009. **48**(10): p. D280-D298.

42. Wang, J., *Recurrent neural networks for computing pseudoinverses of rank-deficient matrices.* SIAM Journal on Scientific Computing, 1997. **18**(5): p. 1479-1493.

43. Lindquist, M.A., et al., *Modeling the hemodynamic response function in fMRI: Efficiency, bias and mis-modeling.* NeuroImage, 2009. **45**(1, Supplement 1): p. S187-S198.

44. Lazar, N.A., *The statistical analysis of functional MRI data*. 2008, Springer: New York. p. xiv, 299 p.

45. Tian, F., et al., *Quantification of functional near infrared spectroscopy to assess cortical reorganization in children with cerebral palsy.* Optics Express. **18**(25): p. 25973-25986.

Biographical Information

Nathan Hervey earned his Bachelors of Science in Mechanical Engineering from Texas A&M University in May of 2009. In the fall of 2011 he began his studies in bioengineering at the University of Texas at Arlington with Dr. George Alexandrakis as his advisor. His research focused on new analysis technique for functional near-infrared spectroscopy data. He hopes to find work in industry as a bioengineer, or possibly pursue a Master of Science degree in computer science.